Proceedings of NHTC'01
35th National Heat Transfer Conference
June 10–12, 2001, Anaheim, California

NHTC01-1413

RAPID IR HEATING OF ELECTRONIC COMPONENTS IN THE TESTING CYCLE

Matthew Sweetland*
Member of ASME
Rohsenow Heat and Mass Transfer Laboratory
Massachusetts Institute of Technology
77 Massachusetts Ave., Room 7-042
Cambridge, MA 02139-4307 USA
sweetlan@mit.edu

John H. Lienhard V
Fellow of ASME
Rohsenow Heat and Mass Transfer Laboratory
Massachusetts Institute of Technology
77 Massachusetts Ave., Room 3-162
Cambridge, MA 02139-4307 USA
lienhard@mit.edu

ABSTRACT

Electronic devices are often tested at elevated temperature after they are manufactured. The time required for testing can be reduced by increasing the rate of heating from ambient to test temperature, particularly if the devices are not removed from their factory carrier trays. This paper describes a new rapid-heating method based on low-cost infrared heaters. A basic model is developed to evaluate the effect of design parameters on temperature uniformity across a component carrier and along the carrier. The model is compared to experimental results.

NOMENCLATURE

A	aspect ratio in view factor calculation
A_{device}	surface area of component (m^2)
B	aspect ratio in view factor calculation
F	radiation view factor
Fo	Fourier number
H	height of chamber wall (m)
I_c	collimated radiation intensity (W/m^2)
I_d	diffuse radiation intensity (W/m^2)
Q_c	surface heat transfer from collimated radiation (W)
Q_d	surface heat transfer from diffuse radiation (W)
Q_T	total surface flux (W/m^2)
T	temperature (°C)
$\overline{T}$	average temperature of a device (°C)
V	velocity of device carrier (m/s)
X	aspect ratio in view factor calculation
Y	aspect ratio in view factor calculation
a	thermal diffusivity (m^2/sec)
c_p	specific heat (J/kg·K)
dA	element of surface area of device (m^2)
k	thermal conductivity (W/m·K)
m	mass of a device (kg)
n	index in Fourier series
t	time (s)
t_c	plane thickness of device carrier (m)
x	position variable in temperature distribution (x)
α	absorptivity
ε	emissivity
λ_n	eigenvalue
ρ	reflectivity

*Author to whom all correspondence should be addressed.

Introduction

In the electronic component manufacturing industry, most components are subjected to a full functional test before they are sold. Depending on the type of components, these functional tests may be performed at room temperature, at cold temperature, or at high temperature (-50°C to 160°C) depending on the type of component and intended market[1] (Pfahnl et al., 1998a; Pfahnl et al., 1999). One of the inherent problems in testing at elevated temperature is the time required in bringing the components to test

[1]Under the hood automotive, aviation, and military components tend to be tested at the temperature extremes.

temperature and returning them to room temperature after testing. Currently, for device carriers holding a large array of components, thermal soak/de-soak chambers are used in the component handlers to raise or lower the device and carrier temperatures. These chambers tend to be large and very slow in conditioning the devices, so the actual time required to electrically test a component is very short compared to the total time required for the testing procedure[2]. Increasing the heating/cooling rate is possible by increasing air velocities or introducing turbulators (Pfahnl et al., 1998b), but a practical limit is quickly reached due to limited blower capacity, noise restrictions, and, for some types of carriers, the danger of blowing loose mounted components out of the carrier.

This paper proposes a new method for rapid uniform heating of multiple components using infrared radiation. Infrared heating is not a new technology and has found broad application ranging from the drying of pulp in the paper manufacturing (Pettersson and Stenström, 2000) to preheating plastics in vacuum molding (Kalpakjian, 1995). Radiant IR heating has also been used extensively in the electronics industry, primarily in rapid thermal processing (RTP) systems, which use radiation for heating materials for CVD and ion implantation. These systems require very high heating rates ($\sim 200°$C/sec), are designed to produce material temperatures up to $1100 - 1200°$C (De Keyser and Donald, 1999), and can be critically affected by temperature distributions within components during heating. The system proposed in this paper for heating devices in the testing process has significantly different objectives than RTP technology. The primary goals are a low cost system, a small system footprint, and the capability to heat multiple encapsulated devices to a uniform final temperature no higher than $160°$C. The proposed method passes a carrier with multiple devices beneath the output of a single quartz-tungsten bulb having a prescribed radiation intensity.

Two main challenges arise in heating components using this method, both of which involve heating components in different positions on the carrier to the same temperature. The first problem is to hold a uniform temperature for all devices along a line perpendicular to the direction of carrier motion. This requirement is not generally a problem if there are only 1–2 components across the carrier, but, for situations with 3 or more components, it is harder to keep the edge components at the same temperature as the central components. This problem can be addressed by suitable selection of the radiant heater, surface properties, and geometry of the thermal chamber, so that the radiation field is uniform across the device carrier.

The second challenge in producing uniform device temperatures is in heating a device on the leading edge of the carrier to the same target temperature as a device on the trailing edge of the carrier. This problem is solely a function of the carrier type. For low conductivity carriers with high thermal resistance between the device and carrier, such as plastic trays with loose mounted devices or polymer-sheet strip carriers, conduction along the carrier does not have to be considered, and leading-edge and trailing-edge devices are easily heated to the same temperature without additional thermal control. For high conductivity carriers, such as lead-frame strip carriers and metal transport trays, conduction along the carrier can cause trailing-edge devices to be heated to a higher temperature than leading-edge devices. Under final steady state conditions, the temperatures of trailing and leading-edge devices will be the same, but the transient effect of carrier conduction must be analyzed to prevent overheating of components and to minimize the settling time after exiting the IR heating system.

[2]Conventional heating systems make take 20-60 minutes to preheat components, depending on the final temperature and component type, while the actual electrical test may only last a few seconds.

Modeling

Three parts are involved in modeling the heating of devices using an IR source. One part is associated with the heating of the actual devices, another with the heating of the device carrier, and the third is associated with the coupling between the carrier and the devices. The main objectives of the modeling are to determine the feasibility of obtaining uniform device temperatures and to determine the parameters that are critical to the final design.

Component Heating

The radiant heat transfer from the IR source to an individual device can be calculated using traditional resistance network methods, but the method must be modified in order to account for the effect of collimating reflectors on the radiation field. Figure 1 shows a cross-sectional view of a proposed heating chamber and Fig. 2 presents an isometric view of the heater and carrier. To keep the size of the heating system to a minimum, the heater is assumed to be the same width as the carrier. Rather than analyzing the IR source and parabolic reflector, the emitted radiation from the IR bulb is separated into a diffuse and collimated component. The IR bulb and reflector assembly can then be treated as an imaginary surface with two specified radiant fluxes, one collimated and the other diffuse. The ratio of collimated to diffuse radiation will depend on the design and reflectivity of the parabolic mirror and the placement of the bulb. The radiant intensity from the bulb can be assumed uniform around its circumference. Then, if a parabolic reflector with the bulb set deep inside the reflector is used, the majority of the emitted radiation will intersect with the reflector and will be reflected as collimated radiation. Conversely, for a very shallow reflector surface, most of the radiation will be diffuse with only a small fraction of the total emission intersecting the reflector surface and becoming collimated. The position of the bulb and reflector are generally fixed for a given design, and the ratio of collimated to diffuse radiation cannot easily be changed. Modeling will be used to evaluate the effect of various collimated/diffuse ratios, but a good starting baseline is to assume half is diffuse and half is collimated. The radiation emitted from

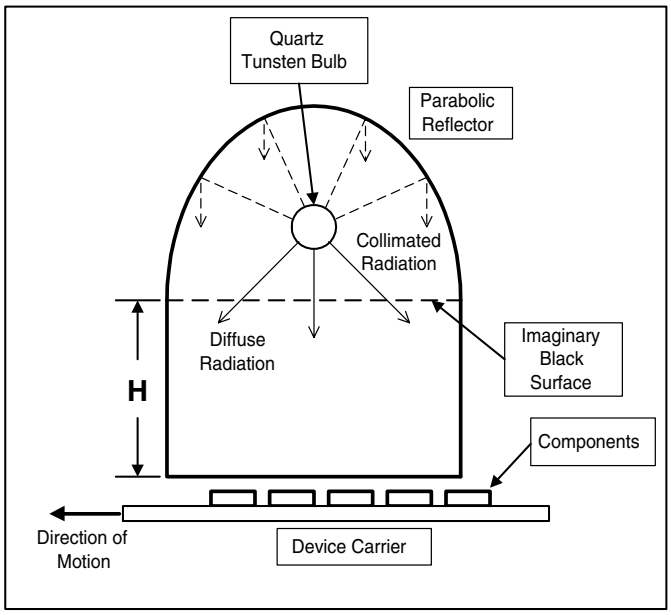

Figure 1. CROSS SECTION VIEW OF PROPOSED IR CHAMBER.

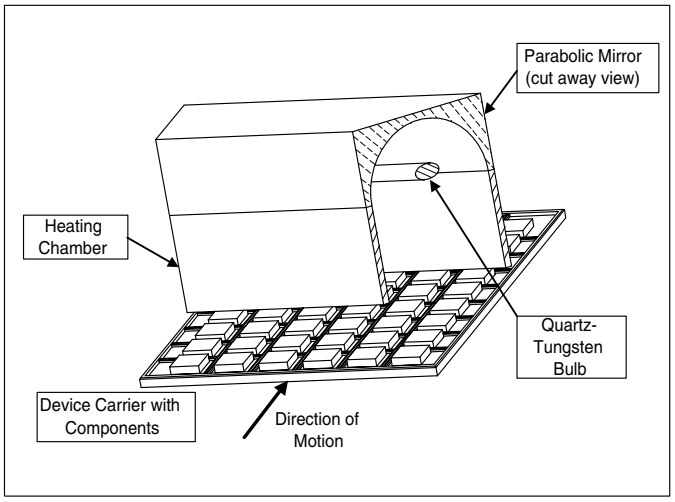

Figure 2. ISOMETRIC VIEW OF IR CHAMBER.

the bulb is also assumed to be uniform over the entire width of the heating chamber[3].

View factors between a device and all surrounding surfaces can be easily calculated for parallel surfaces using

$$F_{dA-1} = \frac{1}{2\pi}\left[\frac{A}{\sqrt{1+A^2}}\tan^{-1}\frac{B}{\sqrt{1+A^2}} + \frac{B}{\sqrt{1+B^2}}\tan^{-1}\frac{A}{\sqrt{1+B^2}}\right] \quad (1)$$

where $A = a/c$, $B = b/c$, and a and b are the dimensions of the wall, and c is the distance between the small area and one corner of the wall (Modest, 1993). For perpendicular surfaces, the view factor can be calculated from

$$F_{dA-1} = \frac{1}{2\pi}\left[\tan^{-1}\frac{1}{Y} - \frac{Y}{\sqrt{X^2+Y^2}}\tan^{-1}\frac{1}{\sqrt{X^2+Y^2}}\right] \quad (2)$$

where $X = a/b$, $Y = c/b$, a is the height of the wall, b is the width, and c is the horizontal distance between the lower corner of the wall and the center of the small area dA (Modest, 1993). The side walls of the chamber are assumed vertical with uniform emissive/reflectivity properties.

These view factor calculations are valid for radiation transfer between a small surface and a parallel or perpendicular surface with one corner in line with the center of the small area. Based on the position of the device, the surrounding surfaces were broken up into rectangular segments such that one corner of each segment[4] was in line with the center of the small area dA. The device was broken into a number of small sections whose area is much smaller than any single wall section and the total view factors were found by discrete integration over the entire component surface to the surrounding segmented surfaces. With all view factors known, the total energy transfer from collimated and diffuse radiation can be calculated. Heat transfer from the collimated radiation is simply given by

$$Q_c = \alpha A_{\text{device}} I_c \quad (3)$$

where A_{device} is the component surface area exposed to the radiation field, α is the device absorptivity, and I_c is the collimated radiation intensity. Heat transfer to the device from diffuse bulb radiation can be combined with radiant exchange between the device and the chamber walls, and the total heat flow can be found using a traditional resistance network. In the resistance model, the imaginary surface in Fig. 1 is treated as a black surface at the same temperature as the component, but with a specified radiant emissive power (i.e., there is no loss from the device to the imaginary surface, but the imaginary surface has a specified flux). The assumption of a black surface neglects the higher intensity directly under the bulb, but this effect is mitigated by an imperfect parabolic reflector surface and the fact that the bulb is not a true line source at the focus of the parabola[5]. Solution of the resis-

[3]The end effects of the bulb are neglected.

[4]Each of the four side walls was broken into two segments to enable use of Eqn. 1 and Eqn. 2.

[5]Higher intensity directly under the bulb will affect final device temperature, but will have a limited effect on temperature uniformity across the carrier.

tance network will not be detailed in this paper, as it is described in most introductory heat transfer texts (Lienhard and Lienhard, 2000; Mills, 1995).

The devices are assumed to be flat with no interaction between adjacent devices and no exposed edges. For any given position within the heating chamber, all view factors can be calculated and the total heat transfer to a device can be found as the sum of the collimated heat transfer and the diffuse heat transfer. Each chamber wall is assumed to be a diffuse isothermal surface with specified emissivity and reflectivity. The temperature of each wall can be set independently. The collimated radiation is assumed to have no secondary effects on energy transfer to the devices[6]. By breaking the progress of a device through the heater as a series of small discrete steps, the heat transfer at each position in the heating chamber can be calculated, and the device temperature may be found from

$$mc_p \frac{d\overline{T}}{dt} = Q_c + Q_d \tag{4}$$

where Q_c is the heat transfer from the collimated radiation, Q_d is the heat transfer from the diffuse radiation and interaction with chamber walls at each position, m is the component mass, c_p is the specific heat, t is the time elapsed since entering the chamber, and $\overline{T}$ is the average temperature of the component. The devices are assumed short in comparison to the width of the heater, so conduction effects along each device do not have to be considered. Entrance and exit effects are treated by assuming partial shielding of each device, i.e. only a fraction of the surface area is exposed to the radiation field. This area is incrementally increased or decreased as the device enters/exits the heating chamber until the device is fully exposed or fully shielded. The diffuse radiation transfer Q_d is a function of the component temperature as this term contains radiant transfer between the device and the walls. The component temperature used in this calculation is the device temperature from the previous step. Convective heat transfer to or from the device while in the heating chamber is neglected. The magnitude of convective transfer is very small in comparison to radiation, and the main interest in this study is the effects of parameters on the radiant heating of the system[7].

A finite difference computer model was constructed using this method to analyze the effects of various heater geometries and other physical parameters on the temperatures of components across a carrier. Of main interest is a comparison of the temperature rise of a component on the edge of a carrier to that of a component in the middle of the carrier. The standard component selected for the simulation is a plastic encapsulated 10 mm QFP[8] device. This device consists of a silicon die mounted on a 0.5 mm thick copper heat spreader with 1 mm of plastic encapsulant on top surface of the device and 0.5 mm of plastic encapsulant on the bottom surface. The radiation intensity for the collimated radiation and diffuse radiation was set at a representative output of 70 kW/m^2 with a constant carrier velocity of 1.0 cm/sec.

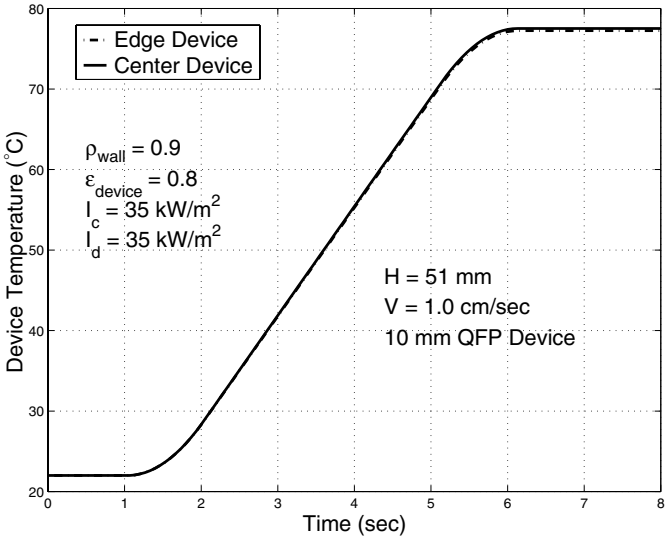

Figure 3. AVERAGE DEVICE TEMPERATURE FOR A 10 mm QFP PACKAGE WITH HIGH REFLECTIVITY CHAMBER WALLS.

While the absolute values of the radiation intensity and carrier velocity will affect the final temperature of the device, of interest is their effect on the temperature difference of devices across a carrier. This means the parameter of interest is the ratio of the collimated to diffuse radiation. Other parameters that can affect the temperature difference between components is the height of the heating chamber[9], the wall reflectivities and temperatures, and the collimated/diffuse intensity ratio. All devices are assumed to be at an initial uniform temperature with uniform radiation properties. Weed and Kirkpatrick (1996) have estimated the emissivity of a plastic encapsulated QFP package as $\varepsilon \approx 0.8$. The QFP package is assumed to be a grey body with $\varepsilon = \alpha$.

Figure 3 shows the average temperature response of two devices, one on the edge of the carrier, one at the center. This figure is for the case with wall reflectivity of 0.8, wall temperatures of 27°C on the two side walls and one end wall, and a wall temperature of 77°C on the remaining wall[10]. The chamber dimensions are 150 mm wide by 41 mm deep by 51 mm high. As can be seen, the edge and center devices are at almost identical temperatures.

[6]Primary and secondary reflections of the collimated radiation are neglected. The collimated radiation is assumed to have no interaction with the chamber walls.

[7]There will be some air flow in actual systems from the hot chamber which will help in the heating of components, but this effect is neglected in order to focus on the maximum heating rate from the radiation source.

[8]Quad Flat Package - 10 mm by 10 mm square.

[9]While the height of the chamber can be modified, the depth of the chamber in direction of motion and width of the heater are assumed fixed.

[10]These wall conditions match the expected external conditions on each wall. Three walls are subject to an ambient environment, while the fourth wall is subject to hot chamber target temperature (in this case 77°C.

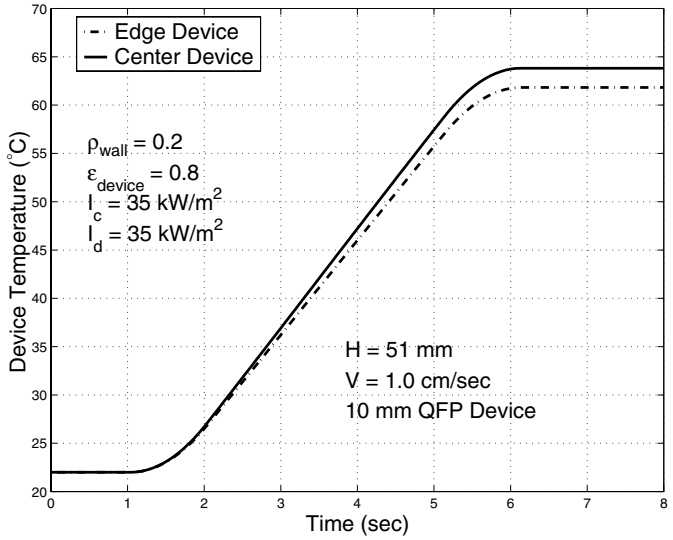

Figure 4. AVERAGE DEVICE TEMPERATURE FOR A 10 mm QFP PACKAGE WITH LOW REFLECTIVITY CHAMBER WALLS.

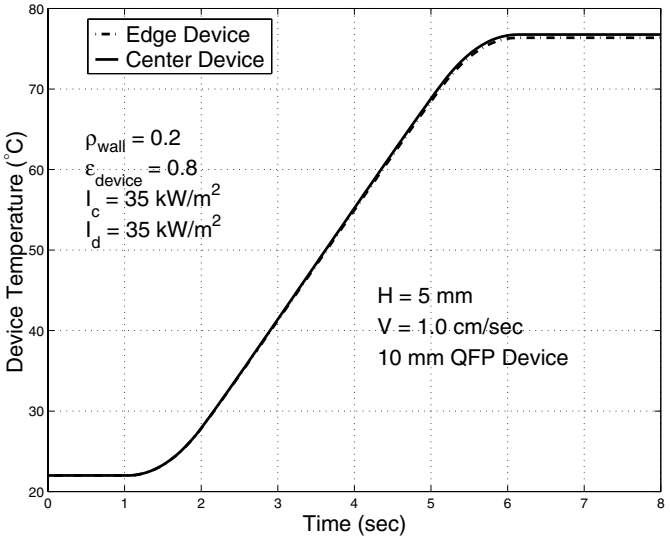

Figure 5. AVERAGE DEVICE TEMPERATURE FOR A 10 mm QFP PACKAGE WITH A 5 mm SIDE WALL HEIGHT AND LOW WALL REFLECTIVITY.

Figure 4 presents data for the same parameter values, but with the wall reflectivity changed from 0.8 to 0.2. Two main effects can be observed from reducing the wall reflectivity while keeping all other parameters the same. The final component temperature is reduced and there is now about a 3°C difference between the edge device and the center device. This shows that from a pure efficiency perspective, high reflectivity walls are preferred to increase the fraction of radiant power that is transferred to the components and to keep the chamber walls at a lower temperature.

Figure 5 presents the simulation results for the case where the wall height is reduced to 5 mm with low reflectivity. As is expected, when the side walls are almost eliminated, reflection effects no longer matter and there is very low absorption by the walls, so the device temperatures are more uniform and the final temperature is close to the case with high reflectivity walls. Figure 6 presents the results for a high ratio of diffuse to collimated radiation, and Fig. 7 presents the results for a low diffuse/collimated ratio. Both sets of results are for low reflectivity walls ($\rho = 0.2$) with a wall height of 51 mm. These results demonstrate that under the assumption that end effects of the IR bulb can be neglected and that output is uniform across the width of the chamber, rapid uniform heating of multiple component is possible with the best results obtained for high reflectivity walls with small distances between the devices heater surfaces. The physical implementation of the assumption to neglect bulb end effects will be discussed in the apparatus section.

Equation 4 illustrates another factor that must be considered in the analysis of component heating using IR radiation. Very high heat fluxes are possible at the surface of the device, so conduction through the device must be considered. While Eqn. 4 will provide information about the average temperature of a component as a function of position in the heating chamber, it does not describe the temperature distribution within the device. This becomes especially important in plastic encapsulated devices where

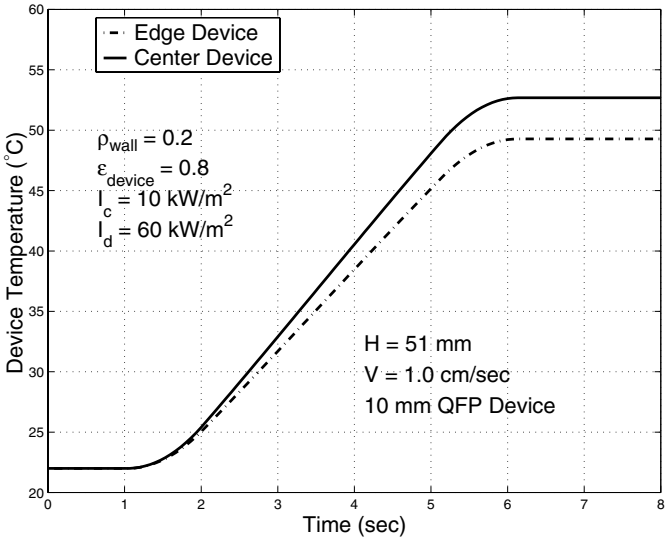

Figure 6. AVERAGE DEVICE TEMPERATURE FOR A 10 mm QFP PACKAGE WITH A LARGE DIFFUSE TO COLLIMATED RADIATION INTENSITY RATIO.

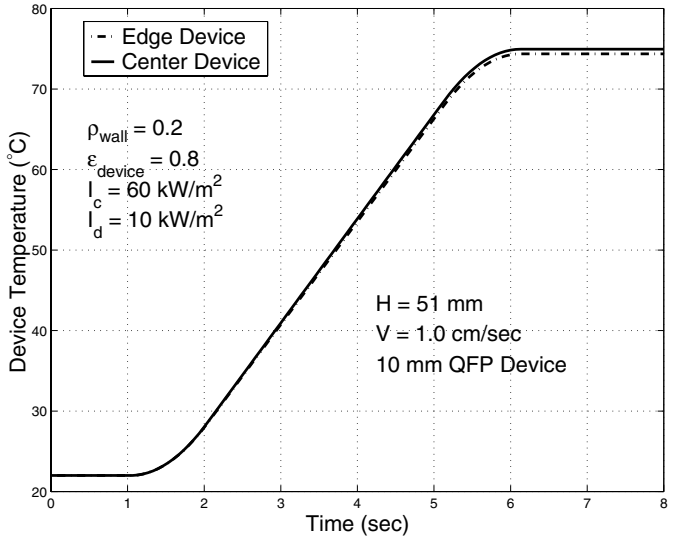

Figure 7. AVERAGE DEVICE TEMPERATURE FOR A 10 mm QFP PACKAGE WITH A SMALL DIFFUSE TO COLLIMATED RADIATION INTENSITY RATIO.

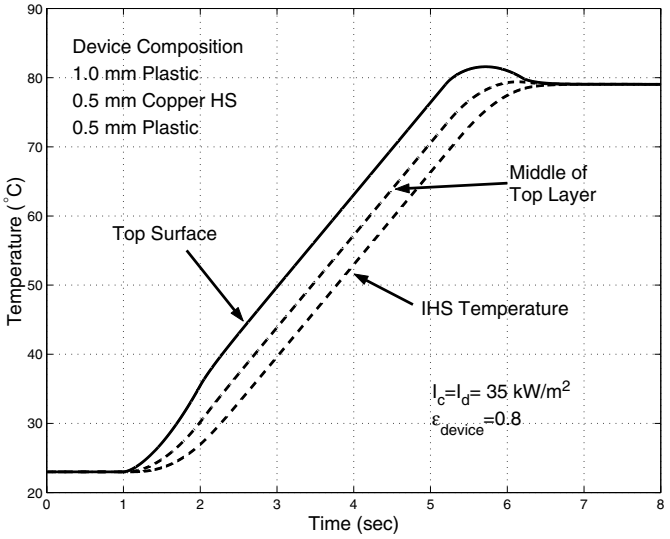

Figure 8. TEMPERATURE RESPONSE INSIDE A 10 mm QFP PACKAGE FOR SPECIFIED SURFACE FLUX.

conduction resistances are very high. To prevent high thermal stresses or material overheating, the conduction through a device must be analyzed.

A typical component will consist of a die, substrate, an encapsulant, and sometimes an integral heat spreader. The die and substrate can be considered a single thermal mass at uniform temperature, so the problem can be effectively reduced to an analysis of three plane layers subject to a specified surface flux. Transient analysis can be simplified by assuming a constant surface flux and no lateral conduction and by the assumption that the die and substrate are a single thermal mass with uniform properties. Contact resistances between the layers are also neglected, and the back face of the composite slab is considered adiabatic.

The solution to this transient problem does not have a compact closed form solution, so an explicit finite difference model was generated to calculate the temperature profile throughout a device. Each material layer was broken into multiple layers, and the temperature at each layer was calculated for a given time step, accounting for surface flux and conduction between layers. The time step in the model was progressively reduced until the quasi-steady state temperature difference between the surface temperature and center die temperature changed by less than 0.5% for a factor of two reduction in time step. An analysis of the 10 mm QFP device before illustrates how large the temperature difference between the surface and die temperature can become. The explicit FDM model was used to generate the temperature profile for a device as it travels through the IR heater. The results are presented in Figure 8. Under these conditions, the surface temperature of the device reaches a higher temperature than the die/substrate. These results are for the 10 mm QFP package which has 1 mm of plastic encapsulant, a 0.5 mm copper heat spreader on which the die is mounted, and a bottom layer of 0.5 mm of plastic encapsulant.

Carrier Heating

To determine the temperature distribution in a device carrier, an approach similar to that for component heating can be used. View factors for any given section of carrier to the surroundings can be calculated and used in a finite difference model to determine the temperature distribution in the carrier. With low conductivity carriers, the effect of conduction along the tray can be completely neglected, and the trailing edge of the carrier will be brought to the same temperature as the leading edge. For high conductivity carriers, the trailing edge of the carrier can potentially end up at a higher temperature than the leading edge owing to conduction along the carrier, potentially bringing the trailing devices above maximum temperature limits.

An implicit finite difference model was developed for calculating the temperature distribution in the carrier. This permits easy definition of changing boundary conditions over the entire length of the carrier. For any given incremental length of the carrier, the total radiant heat transfer can be calculated in a manner identical to the component heating method. This surface flux over an incremental length was combined with conduction effects to calculate the temperature distribution in the tray as it traveled through the heater. Convection from the carrier to the surrounding environment was neglected. Figure 9 demonstrates that, for

a low conductivity carrier, the temperature along the carrier remains fairly uniform. Figure 10 shows the results for a high conductivity[11] carrier. Obviously, high conductivity carriers present the additional problem of a non-uniform temperature distribution along the carrier after exiting the heating chamber.

Like the devices themselves, low conductivity carriers will have a large temperature difference across the thickness of the carrier. Calculation of this temperature profile is easier to determine in closed form than component profile because there is a single material layer. Assuming an adiabatic back face and no temperature gradients in the lateral directions, the temperature profile within the device can be calculated from (Carslaw and Jaeger, 1959)

$$T(x) = \frac{Q_T t_c}{k}\left[\frac{x^2}{2t_c^2} - \frac{1}{6} + \mathrm{Fo} + \frac{2}{\pi^2}\sum_{n=1}^{\infty}\frac{(-1)^n \cos(\lambda_n x)\exp^{-\lambda_n^2 at}}{n^2}\right] \quad (5)$$

where x is measured from the back (adiabatic) surface of the carrier, t_c is the carrier thickness, k is the thermal conductivity, $\mathrm{Fo} = at/t_c^2$ is the Fourier number, and $\lambda_n = n\pi/t_c$. Again, the maximum temperature will occur at irradiated surface ($x = t_c$). This analysis yields the worst case profile, as actual carriers are not 1-D and lateral conduction into side ribs and sections of the carrier that are shielded from the radiation by the components will lower the actual maximum carrier temperature, but it helps to identify the maximum allowable heating rate.

Device/Component Coupling

The final temperature of the components is a function of both the heat transfer to the individual devices and the heat transfer to the carrier. In cases where the majority of the thermal mass is associated with either the components or the carrier, the final temperature will be driven by that thermal mass. In cases where the thermal masses are more evenly distributed, a full analysis of the energy transfer to all parts is required to determine the final temperature of the components. For situations where either the carrier or the components drive the final temperature, the heat transfer to the other side must be analyzed to ensure that maximum temperature limits are not exceeded. The time required to establish final steady state equilibrium between the carrier and components will vary depending on component type, type of mounting (loose mounted, hard wired, etc.), and initial temperature difference after exiting the heater. The more uniform the temperature profile when exiting the heater, the less time required to reach steady state. The final, steady state temperature can be found through a simple energy balance.

[11] Cast aluminum carrier.

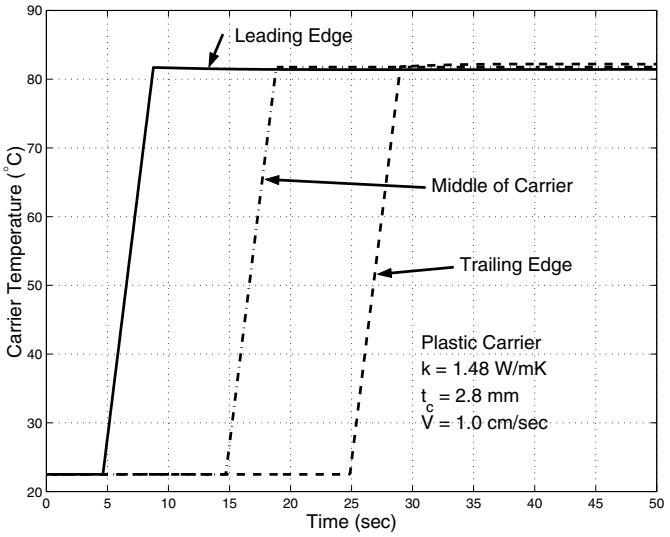

Figure 9. TEMPERATURE PROFILE FOR LOW CONDUCTIVITY CARRIER.

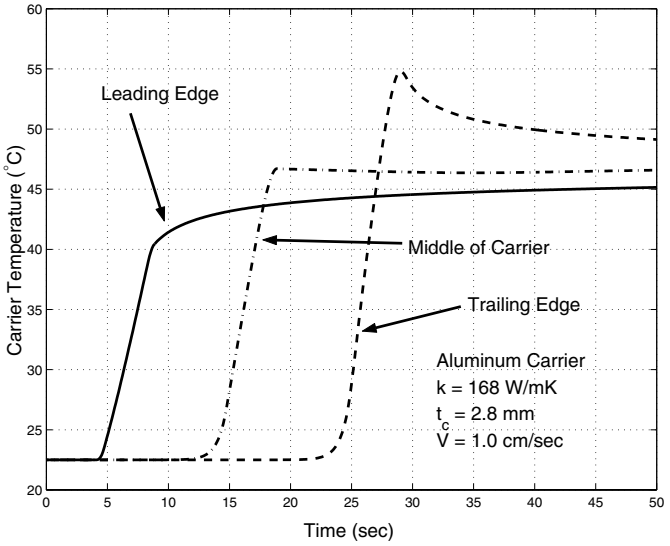

Figure 10. TEMPERATURE PROFILE FOR HIGH CONDUCTIVITY CARRIER.

Apparatus

The main goal in the design of a component heating system is raise all devices to a uniform temperature. Modeling has demonstrated that uniform heating across the width of the heater can be obtained under the assumption that bulb end effects can be eliminated. One method of meeting this condition is to use a bulb that is much longer than the width of the carrier; how-

ever, IR bulb sizes and shapes are limited, and using a radiation source that is much larger than the tray is inefficient in terms of energy and space utilization. Another possible implementation is to use multiple bulbs arranged so as to provide a uniform radiation field, but this can be very difficult in practice, requiring ray tracing over multiple reflections for the full emission from each bulb. The problem cannot be solved in reverse, starting from a uniform flux and working backwards to a bulb arrangement, so the problem becomes one of repeated experimental analysis.

A third option exists in the selection of an IR source. By chosing a bulb that is slightly longer than the width of the carrier, the heating chamber and mounting system can be designed so that output from the ends is shielded from the components and carrier. This can be done fairly easily with edge reflectors that extend up to the bulb surface and by putting radiation absorbing surfaces beneath the ends of the bulb assembly. This method was chosen for construction of a prototype system.

IR Source Selection

The characteristics of the radiation are dependent on the generating materials (i.e. filament type), the design operating temperature, and any filtering elements such as gases and bulb materials. The bulb chosen is a quartz-tungsten bulb, 9.5 mm in diameter and 254 mm in total length[12] with a maximum filament temperature of 2227°C and a peak wavelength of $1.15\ \mu$m. Bulb life is estimate at 3000 hrs with a response time of 3 seconds for 90% of full operating temperature from a cold start. A short wavelength IR source was chosen because the response time is much faster than traditional long wavelength systems.

The system output is adjustable from zero power to full power using an adjustable voltage supply. Actual radiant power of the system is not precisely known, nor is it of critical importance. Final temperatures are selected by making several runs at multiple power levels and then using this to develop a correlation to find the set point for the desired temperature. There is sufficient uncertainty in the radiant properties (emissivities, radiant intensities, etc.) that absolute determination of final temperature is not practical without some form of calibration test.

Heating Chamber Design

The IR chamber must be designed around the bulb type and carrier component configuration. The main goal in design of the chamber is to obtain high reflectivities and prevent bulb end effects from affecting the radiation field. End reflectors were custom fit to extend up into the parabolic reflector section with a very small gap left between the reflector and surface of the bulb. The heating chamber was constructed with a 0.2 mm layer of aluminum foil over a 8 mm high temperature millboard insulating layer to reduce external losses. The height of the heating chamber was kept to a minimum, but physical mounting requirements forced a minimum

[12] Includes electrical connections.

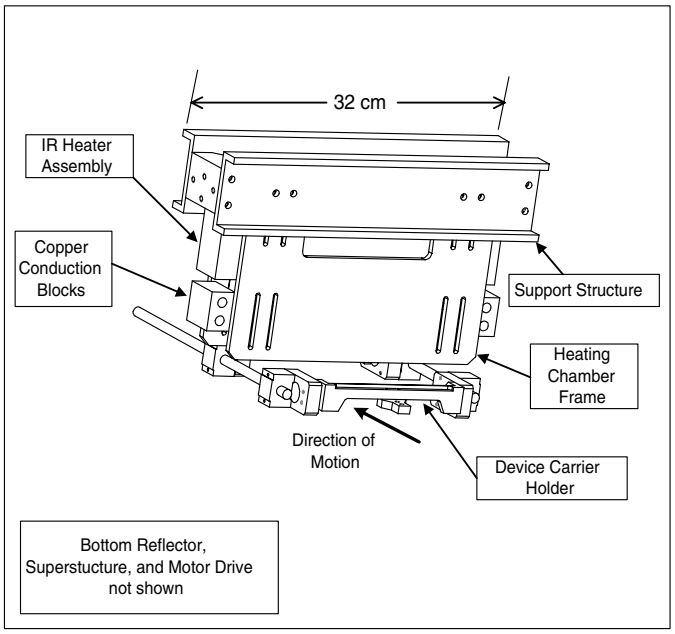

Figure 11. IR HEATING CHAMBER ASSEMBLY.

height of 51 mm. The analytical model shows this is not a problem as long as the wall reflectivity is kept high. At the peak wavelength of the IR bulb, the aluminum has a reflectivity on the order of 0.90–0.95 (Mills, 1995). The entire reflector/insulator assembly was supported by an aluminum box frame. Copper shields with low reflectivity surfaces were installed below the bulb sections outside of the heating chamber. The absorbed radiant energy from the end sections of the bulb was conducted through the copper shields to be dissipated to the environment through external heat sinks with integral fan units. Figure 11 shows a view of the assembled IR system without the motor drive and without a carrier installed. Also not shown are the base reflector unit and the integral fan heat sinks mounted on the end of the copper shields.

The carrier was mounted on thin black-anodized aluminum cross bars supported on linear bearings. The bearings were mounted on a pair of linear rails and the whole system was moved using a lead screw and variable speed motor assembly. Only a very thin section of the supporting aluminum structure is exposed to the radiant energy, with all bearings, mounts and drive components operating outside the radiation field. The base of the heating chamber was lowered to within 1 mm of the component/carrier surface to reduce external losses, and an aluminum reflector was mounted below the heating chamber with just enough separation to allow the carrier to pass. The carrier travels from open air, through the heater, and into a low volume insulated delivery chamber. The inside of the delivery chamber was lined with polished aluminum to reduce radiant losses between the components and the chamber. The delivery chamber is not currently set up

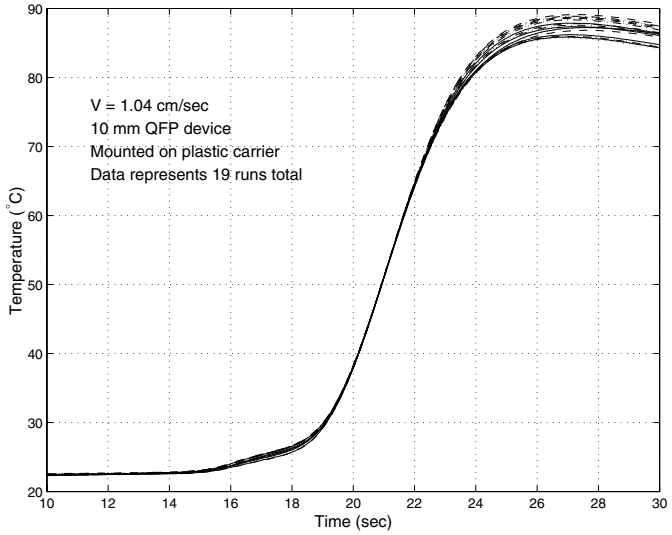

Figure 12. EXPERIMENTAL DATA FOR TESTING LATERAL HEATING UNIFORMITY WITH HIGH REFLECTIVITY WALLS . DATA IS FOR COMPONENT MOUNTED ON CARRIER CENTERLINE. TEMPERATURE MEASURED ON INTEGRATED HEAT SPREADER.

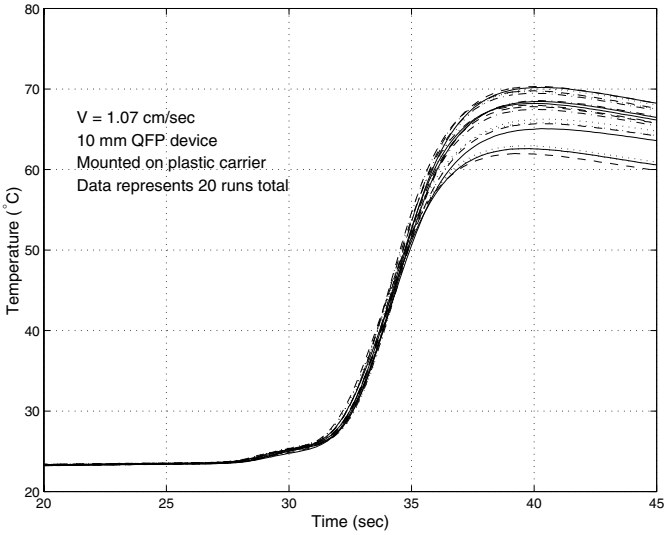

Figure 13. EXPERIMENTAL DATA FOR TESTING LATERAL HEATING UNIFORMITY WITH LOW REFLECTIVITY WALLS . DATA IS FOR COMPONENT MOUNTED ON CARRIER CENTERLINE. TEMPERATURE MEASURED ON INTEGRATED HEAT SPREADER.

to be preheated to the target temperature, but a system is being developed to allow this capability.

Experimental Results

A number of experiments have been run, focused on the heating of 10 mm QFP devices in a plastic carrier and on the heating of a plane aluminum carrier without any devices. The QFP plastic carrier has 6 components mounted across the width of the carrier, with 16 rows of devices along length the carrier.

Figure 12 shows the results for multiple runs through the heater in all lateral positions. As can be seen, the final temperatures are within a range of 3°C for all runs. This data is for a heating chamber height of 51 mm, a heater width[13] of 41 mm, a carrier velocity of 1 cm/sec, and aluminum foil coated walls with a reflectivity of 0.9. Some of the variation can be explained through uncontrolled convection conditions and instrumentation errors, but even discounting these factors, the final temperature is very uniform and well within the ± 3°C that is often specified for thermal conditioning systems in electronic test handlers. Figure 13 shows data for an identical system as with Fig. 12 but with low reflectivity walls[14] A comparison of experimental data to the simulation can been seen in Fig. 14. The simulation data in this figure was generated by using data from the model for heating of a device in the IR chamber to generate a flux versus time data

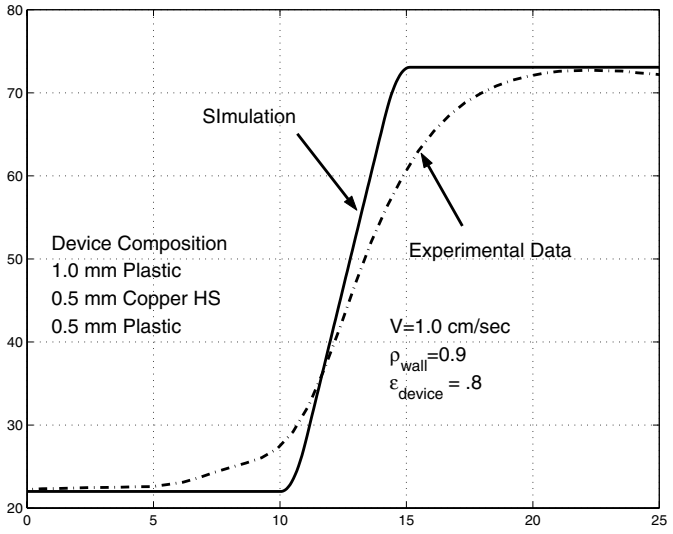

Figure 14. EXPERIMENTAL AND SIMULATION DATA FOR 10 mm QFP ON CARRIER CENTERLINE.

set. This data set was then used in the explicit FDM model for heating of a composite slab to generate the temperature profile of the device IHS as a function of time. The initial heating of the experimental device compared to the simulation is due to radiation leakage outside the heating chamber. The experimental data shows a slower response than the simulation indicating that the

[13] Heater width is fixed for all runs.

[14] Polished aluminum walls were replaced with hard black anodized aluminum - $\rho \sim 0.5$.

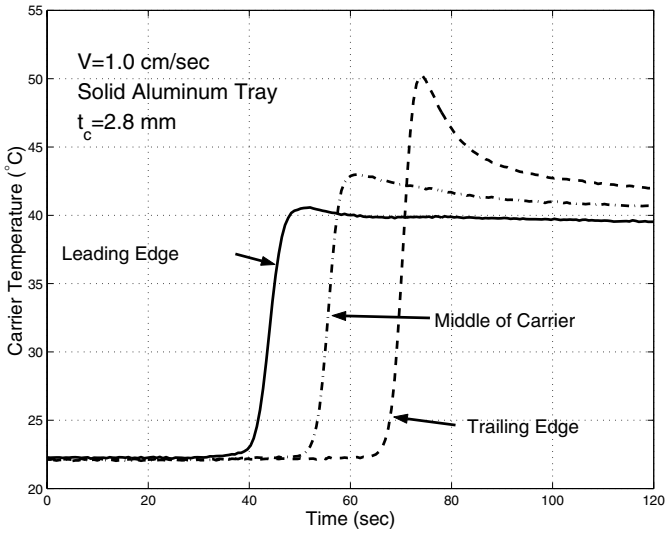

Figure 15. TEMPERATURE PROFILE FOR HIGH CONDUCTIVITY CARRIER.

conduction resistance is higher in the actual case than in the model. This may be due to interfacial resistance between the layers that was not included in the model, or it may be that the conductivity of the plastic encapsulant is lower than believed, or it may be the result of an instrumentation problem where the temperature is being sensed at a point just below the QFP's heat spreader.

Experimental measurements of the effect of conduction along the carrier are presented in Fig. 15 for a 2.8 mm thick flat aluminum carrier. As predicted, the trailing edge temperature is significantly higher than the leading edge temperature. This demonstrates the importance of considering the conduction along the carrier in calculating the peak and steady state temperature profiles in the carrier.

Error Analysis

The data presented in Fig. 12 thru 15 were obtained using T type thermocouples with a 6 channel PCMCIA DAQ card with built in cold junction reference. The precision of the absolute temperature measurements is only $\pm 2°$C, but of more interest in this work is the resolution and repeatability for a change in temperature. For the the T type thermocouples used and the associated DAQ system, single channel repeatability is within $\pm 0.5°$C. To reduce the error for testing of uniform heating across the carrier, the same device was used at each position over multiple runs. This reduces the error due to instrumenting each component at the exact same point and eliminates variability in contact resistance values. The output from the IR bulb was held constant between runs by securing the controller setting at an initial fixed value. Limited information is currently available on the variability of the IR output, but initial estimates put repeatability at $\pm 0.5\%$ of a given fixed output.

Carrier velocity was measured using a hand held digital tachometer on the output shaft from the motor, before reduction through a fixed ratio gear transmission. Accuracy of the tachometer is specified as ± 0.5 rpm, but measured variation of the motor during a run is over ± 10 rpm. For a 10:1 gear ratio and a 2 tpi precision ground lead screw, this corresponds to a velocity variation of ± 0.02 cm/sec.

For these conditions, a standard propagation of error method (at 95% confidence levels) can be used to estimate the expected variation in temperature change for a given component. Since the errors in the IR flux and carrier velocity are independent, and since the total temperature change of a device can be estimated from $\Delta T = Q_a t / m c_p$ where Q_a is an average flux and t is the effective residence time in the heater, the expected variation in temperature change can be calculated as

$$\frac{\delta \Delta T}{\Delta T} = \sqrt{\left(\frac{\delta Q_a}{Q_a}\right)^2 + \left(\frac{\delta t}{t}\right)^2} \tag{6}$$

This will yield an expected variation of $\pm 2.1\%$ of ΔT for a carrier velocity of 1 cm/sec at any Q value. For the data in Fig. 12, this represents an expected variation of $\pm 1.2°$C, which is over twice as large as the repeatability of the thermocouple. This helps explain the variation in the data in Fig. 12.

Future Work

Research on this technology is continuing. The analytical models will be expanded to better couple component heating and carrier heating. A design methodology will be formalized to determine the maximum safe heating rate for any given tray, component configuration, and final temperature. Consideration of losses to carrier transport systems will be included in the model, and the potential effect of thermal radiation on material properties will be considered (i.e., degradation of the plastic encapsulant by radiation).

Experimental work will be performed on high conductivity carrier systems with mounted components and various control methods will be tested. The experimental apparatus will be modified to minimize convective losses on the hot side of the heater, and a process will be developed for estimating the thermal resistance between loose mounted component and the contacting carriers.

Conclusions

A system model has been developed that can predict the temperature uniformity of electronic components subject to rapid infrared heating in which separate models are applied to the heating

of the components and the heating of the carrier tray. A prototype system was assembled based on the model, and temperature uniformity across a device carrier has been confirmed. The predicted effect of conduction along a carrier has also been validated.

The final temperature of the components is a function of both the component heating and the carrier heating. Analysis of temperature profiles through the devices and carriers must be considered to avoid overheating of materials at the irradiated surface. Future work is required to develop a unified model capable of optimizing a heating design for any component configuration.

REFERENCES

Carslaw, H.S., and J.C. Jaeger, *Conduction of Heat in Solids*, 2nd ed. Oxford: Oxford University Press, 1959, §3.8.

De Keyser, Robin, and James Donald III, *Model Based Predictive Control in RTP Semiconductor Manufacturing*, Proc. IEEE Intl. Control Applications Conf., Kohala, Hawaii, 1999.

Kalpakjian, Serope, *Manufacturing Engineering and Technology*, 3rd ed. Reading: Addison-Wesley, 1995.

Lienhard IV, John H., and John H. Lienhard V, *A Heat Transfer Textbook*, 3rd ed., Cambridge, 2000. http://web.mit.edu/lienhard /www/ahtt.html

Mills, Anthony F., *Heat and Mass Transfer*. Chicago: Irwin, 1995.

Modest, Michael F., *Radiative Heat Transfer*. New York: McGraw-Hill Inc., 1993.

Pfahnl, Andreas C., John H. Lienhard V, and Alexander H. Slocum, "Temperature Control of a Handler Test Interface," *Proc. IEEE Intl. Test Conf.*, Washington DC, 1998.

Pfahnl, Andreas C., John H. Lienhard V, and Alexander H. Slocum, "Heat Transfer Enhancing Features for Test-Handler Trays," *IEEE Trans. Comp. Packaging & Manufactgr. Tech. Part C: Manufacturing*, 21:4, 302–310, 1998.

Pfahnl, Andreas C., John H. Lienhard V, and Alexander H. Slocum, "Thermal Management and Control in Testing Packaged Integrated Circuit Devices," *Proc. 34th Intersociety Energy Conversion Conf.*, Vancouver BC, Aug. 1999, Paper No. 1999-01-2723.

Pettersson, Magnus, and Stig Stenström, "Modelling of an Electric IR Heater at Transient and Steady State Conditions Part II: Modelling a Paper Dryer", *Intl. J. Heat Mas Trans.*, 43, 1223–1232, 2000.

Weed, Kevin, and Allan Kirkpatrick, "An Experimental Investigation of the Emissivity of Various Electronic Packages," *Proc. Twelfth IEEE SEMI-THERM Symp.*, 59–64, 1996.

ACKNOWLEDGMENTS

The authors would like to thank Teradyne, Inc. for financial support of this work. The authors would also like to thank Andreas Pfahnl and Ray Mirkhani of Teradyne for their technical support of this work, and Jaynary Baretto of the University of Puerto Rico at Mayaguez for her help in calculating the view factors.